

Improving Factuality of 3D Brain MRI Report Generation with Paired Image-domain Retrieval and Text-domain Augmentation

Junhyeok Lee^{a,*}, Yujin Oh^{b,*}, Dahyoun Lee^c, Hyon Keun Joh^d, Chul-Ho Sohn^{e,f}, Sung Hyun Baik^{e,g}, Cheol Kyu Jung^{e,g}, Jung Hyun Park^{e,h}, Kyu Sung Choi^{e,f,**}, Byung-Hoon Kim^{e,i,j,**}, Jong Chul Ye^{k,**}

^aInterdisciplinary Program in Cancer Biology, Seoul National University College of Medicine, Seoul, Republic of Korea

^bDepartment of Radiology, Massachusetts General Hospital (MGH) and Harvard Medical School, Boston, MA, USA

^cDepartment of Biomedical Systems Informatics, Yonsei University College of Medicine, Seoul, Republic of Korea

^dDepartment of Medicine, the Graduate School of Yonsei University, Seoul, Republic of Korea

^eDepartment of Radiology, Seoul National University College of Medicine, Seoul, Republic of Korea

^fDepartment of Radiology, Seoul National University Hospital, Seoul, Republic of Korea

^gDepartment of Radiology, Seoul National University Bundang Hospital, Seongnam, Republic of Korea

^hDepartment of Radiology, Seoul Metropolitan Government Seoul National University Boramae Medical Center, Seoul, Republic of Korea

ⁱDepartment of Psychiatry, Yonsei University College of Medicine, Seoul, Republic of Korea

^jInstitute of Behavioral Sciences in Medicine, Yonsei University College of Medicine, Seoul, Republic of Korea

^kKim Jaechul Graduate School of AI, Korea Advanced Institute of Science and Technology (KAIST), Daejeon, Republic of Korea

Abstract

Acute ischemic stroke (AIS) requires time-critical management, with hours of delayed intervention leading to an irreversible disability of the patient. Since diffusion weighted imaging (DWI) using the magnetic resonance image (MRI) plays a crucial role in the detection of AIS, automated prediction of AIS from DWI has been a research topic of clinical importance. While text radiology reports contain the most relevant clinical information from the image findings, the difficulty of mapping across different modalities has limited the factuality of conventional direct DWI-to-report generation methods. Here, we propose paired image-domain retrieval and text-domain augmentation (PIRTA), a cross-modal retrieval-augmented generation (RAG) framework for providing clinician-interpretative AIS radiology reports with improved factuality. PIRTA mitigates the need for learning cross-modal mapping, which poses difficulty in image-to-text generation, by casting the cross-modal mapping problem as an in-domain retrieval of similar DWI images that have paired ground-truth text radiology reports. By exploiting the retrieved radiology reports to augment the report generation process of the query image, we show by experiments with extensive in-house and public datasets that PIRTA can accurately retrieve relevant reports from 3D DWI images. This approach enables the generation of radiology reports with significantly higher accuracy compared to direct image-to-text generation using state-of-the-art multimodal language models.

1. Introduction

Stroke is the second leading cause of death and the third leading cause of disability worldwide, as well as a major cause of dementia (Feigin et al., 2022). Acute ischemic stroke (AIS), accounting for approximately 70% of all stroke cases globally, arises from a sudden loss of blood supply to one or more major vessels of the brain (Campbell et al., 2019). Timely intervention of AIS is critical,

*Co-first authors.

**Co-corresponding authors.

Email addresses: ent1127@snu.ac.kr (Kyu Sung Choi),
egyptdj@yonsei.ac.kr (Byung-Hoon Kim),
jong.ye@kaist.ac.kr (Jong Chul Ye)

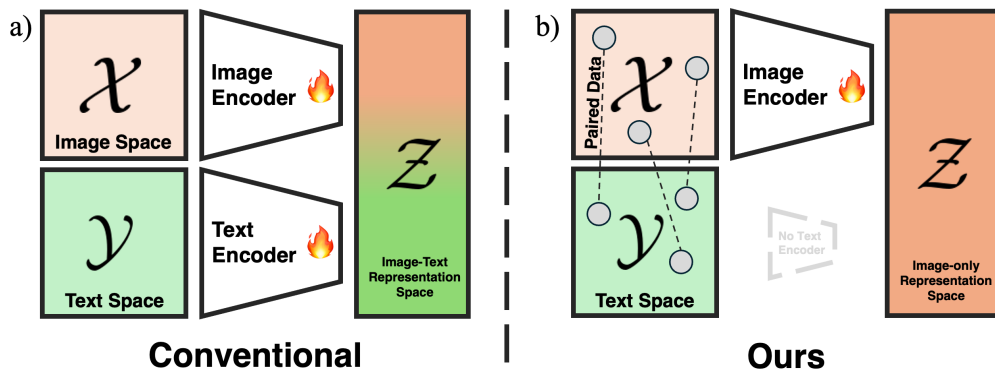


Figure 1: Graphical illustration of the proposed method for image-to-text retrieval. a) Conventional methods require training an image encoder and/or a text encoder to align similar image-text pairs at the representation space, which a significant difficulty comes from learning the cross-domain joint distribution. b) The proposed method requires training only an image encoder to minimize the distance of similar images at the representation space. The relevant text is obtained from the retrieved similar image, which holds paired ground-truth text data that serve as the retrieved text.

as delays in initial treatment can significantly increase the risk of permanent neurological damage and long-term disability. Current stroke management guidelines from the American Heart Association/American Stroke Association (AHA/ASA) emphasize the importance of rapid endovascular intervention within 4.5 to 6 hours of symptom onset to reduce the likelihood of long-term impairment (Powers et al., 2019).

Magnetic resonance imaging (MRI) plays a central role in the diagnosis and management of AIS, providing insights into brain tissue viability and ischemic injury (San Román et al., 2018). Diffusion weighted imaging (DWI) and apparent diffusion coefficient (ADC) are particularly valuable for detecting acute ischemic changes, enabling clinicians to assess both ischemic territories and potential hemorrhagic transformation (Campbell et al., 2019). Accordingly, these MRI findings are essential for corroborating neurological assessments and guiding therapeutic decisions in AIS treatment.

The advent of artificial intelligence (AI) in medical imaging has opened new avenues for automating AIS detection and prediction from brain imaging data (Mouridsen et al., 2020). Most studies to date have focused on predicting ischemic stroke outcomes using deep learning based on DWI. Herzog et al. (2020) proposed a framework for diagnosing ischemic stroke patients that integrates Bayesian uncertainty analysis with Bayesian CNN. This approach yields probabilities and confidence

levels for stroke lesions based on 2D MRI. Cetinoglu et al. (2021) evaluated a CNN model employing transfer learning techniques, achieving stroke detection accuracies of 96% and 93% with modified MobileNetV2 and EfficientNet-B0. Tasci and Tasci (2022) introduced PDRNet, a preprocessing-based model that combines DenseNet and ResNet architectures, achieving classification accuracies ranging from 97.56% to 99.32% using CNNs alongside support vector machine classifiers. Lee et al. (2023a) demonstrated the effectiveness of modified LeNet, Inception-v3, and EfficientNet-B0 in the automatic detection and vascular territory classification of hyperacute staged ischemic stroke using DWI. Koska et al. (2024) showed that incorporating various input combinations, such as edge maps and threshold processing, significantly enhanced the classification accuracy of stroke-affected areas in DWI. While these studies provide meaningful clinical information, there is still a lack of research that aims to directly provide a clinician-interpretative radiological reading report of input MRIs written in a textual format. One recent study (Liu et al., 2023) proposed generating radiological reports by extending segmentation models for AIS in a supervised manner, relying heavily on manual annotation. However, this approach does not fully utilize large language models, resulting in limited scalability and generalizability when applied to various multimodal data.

Radiology reports play an indispensable role in the

clinical workflow for managing AIS (Ong et al., 2020). Clinicians rely on detailed radiology reports generated from DWI images to make informed decisions regarding treatment options, such as thrombolysis or mechanical thrombectomy, which need to be administered within a narrow therapeutic window to maximize patient outcomes (Heo et al., 2020). Automated report generation systems can help reduce radiologist workload, minimize diagnostic delays, and provide more consistent assessments. However, generating accurate radiology reports for DWI images is inherently challenging due to the complexity of the data, which captures both ischemic and non-ischemic tissues in a highly detailed, volumetric format.

The recent development of foundation models has significantly impacted research directions in medical image analysis, by enabling multimodal tasks that integrate imaging data with other data modalities that provide clinical context (Moor et al., 2023). These models, predominantly based on Transformer architectures with a large number of parameters, are trained on diverse datasets to learn their generalized representations (Bommasani et al., 2021). Large language models (LLMs) and vision-language models (VLMs) are now being applied to a range of multimodal medical imaging tasks, such as chest X-rays, computed tomography (CT) scans, pathology slides (Singhal et al., 2023; Lee et al., 2023b; Li et al., 2024). Despite these advancements, the generation of accurate and clinically useful reports from 3D medical images, such as MRI, remains a challenge. This limitation is due to the 1) absence of pretrained 3D medical image encoders and 2) difficulty of aligning cross-modal representations, or bridging the modality gap (Huo et al., 2024; Ma et al., 2024)(Figure 1a). This is particularly evident in the context of AIS, where current off-the-shelf 2D VLMs struggle to generate reliable radiology reports from 3D MRI data (see Section 3.1.2 for baseline results).

Training Vision Transformers (ViTs) from scratch for medical image analysis typically requires large, labeled datasets, a resource that is often scarce in clinical settings (Dosovitskiy et al., 2020). Self-supervised learning (SSL) has emerged as a promising solution, leveraging abundant unlabeled data to improve model performance across various computer vision tasks (Jing and Tian, 2020; Caron et al., 2021). Among these SSL approaches, masked image modeling, such as the masked auto-encoder (MAE), has shown particular success in per-

taining ViTs by masking parts of images and learning to reconstruct them (Xie et al., 2022; He et al., 2022). The SSL techniques, including MAE, also have demonstrated substantial improvements in segmentation and classification tasks with medical images like X-rays, CT (Zhou et al., 2023). In this work, we pretrain a 3D ViT on a large, unlabeled MRI dataset with MAE to serve as a 3D MRI vision encoder and leverage this vision encoder to successfully perform our target multimodal downstream task, the DWI radiology report generation for AIS.

A trivial way to integrate the pretrained 3D ViT for text generation is to leverage the encoder output representation as an input to a pretrained LLM. However, ensuring factual accuracy remains a significant hurdle for such approaches that naïvely integrates the 3D ViT with a pretrained LLM. To address this, we incorporate retrieval-augmented generation (RAG) to enhance the factuality of reports by retrieving relevant information from a validated database during the generation process. RAG is a technique for improving the factuality of an LLM by retrieving relevant information from a verified database to augment the generation process (Lewis et al., 2020). This approach has demonstrated improved accuracy, factuality, and contextual relevance in generated texts, augmenting the knowledge initially encoded in the model during training (Izcard and Grave, 2021; Borgeaud et al., 2022; Karpukhin et al., 2020; Ram et al., 2023). Although RAG has shown success in knowledge-intensive tasks, its application in medical imaging, particularly with 3D data, poses unique challenges not only because of the lack of appropriate 3D vision encoders but also because of the difficulty in cross-modal representation matching for accurate retrieval.

Here, we propose paired image-domain retrieval and text-domain augmentation (PIRTA), a cross-modal retrieval-augmented generation framework for providing clinician-interpretative AIS radiology reports with improved factuality. PIRTA mitigates the need for learning cross-modal mapping, which poses difficulty in image-to-text generation, by casting the cross-modal mapping problem as an in-domain retrieval of similar MRI images from the database that have paired ground-truth text radiology reports (Figure 1b). This novel approach improves the factual accuracy of the generated radiology report by addressing the difficulties inherent in image-to-text generation, particularly for 3D medical images.

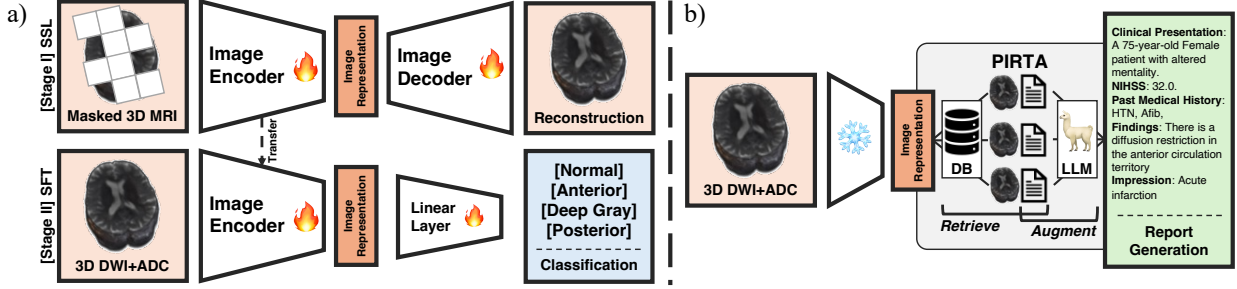


Figure 2: Schematic illustration of the proposed method. a) Overview of training the 3D MRI image encoder. In the first stage, the 3D MRI input images are masked and encoded with a 3D ViT encoder, then decoded to reconstruct the original input 3D MRI image. In the second stage, the pretrained image encoder is fine-tuned to classify the four ischemic territories. b) Overview of the proposed cross-modal RAG framework PIRTA. Parameters of the image encoder are frozen, and the most relevant images and their paired ground-truth radiology reports are retrieved based on the cosine similarity in the image representation space. Retrieved radiology reports are used to augment and improve factuality of the final generated radiology report.

2. Methods

2.1. Problem definition

Let \mathcal{X} represent the space of MRI images and \mathcal{Y} represent the space of radiology reports. The objective of this study is to retrieve an accurate radiology report $y \in \mathcal{Y}$ for a given MRI image $x \in \mathcal{X}$. Traditional approaches aim to solve this problem by learning a cross-modal mapping between the two spaces \mathcal{X} and \mathcal{Y} , typically via two neural network encoders:

$$f_{\text{image}} : \mathcal{X} \rightarrow \mathcal{Z}, \quad (1)$$

$$f_{\text{text}} : \mathcal{Y} \rightarrow \mathcal{Z}, \quad (2)$$

where \mathcal{Z} is a shared latent space between the image and the text. It should be noted that we assume that the image-to-text generation task can be thought of as training a neural network text decoder instead of training the text encoder.

In this setup, the goal is to minimize the distance between the encoded image and text representations in \mathcal{Z} , such that:

$$d(f_{\text{image}}(x_q), f_{\text{text}}(y_j)) \quad (3)$$

is minimized, where $x_q \in \mathcal{X}$ is the query image, $y_j \in \mathcal{Y}$ is the most relevant radiology report, and d is a suitable distance metric (e.g., cosine distance, Euclidean distance).

The challenge with this approach lies in the joint learning of two distinct modality encoders, which introduces significant complexity. This complexity arises from the fact that the joint distribution $P(x, y)$ over images and their corresponding reports must be modeled, which requires learning two conditional distributions: $P(y|x)$ (the mapping from image to text) and $P(x|y)$ (the mapping from text to image).

Formally, let $\mathcal{H}_{\text{image}}$ and $\mathcal{H}_{\text{text}}$ represent the hypothesis spaces for the image and text encoders, respectively. The joint hypothesis space \mathcal{H} is defined as the product of these two spaces:

$$\mathcal{H} = \mathcal{H}_{\text{image}} \times \mathcal{H}_{\text{text}} \quad (4)$$

The complexity of the learning problem is proportional to the combined complexities of $\mathcal{H}_{\text{image}}$ and $\mathcal{H}_{\text{text}}$. Using a suitable non-negative complexity measure $C(\cdot)$, such as VC dimension, Rademacher complexity, or covering numbers, we can express the total complexity as:

$$C(\mathcal{H}) = C(\mathcal{H}_{\text{image}}) + C(\mathcal{H}_{\text{text}}). \quad (5)$$

Given that both encoders need to be trained jointly to align image and text representations, the cross-modal learning task has high complexity, especially when dealing with volumetric medical images like 3D MRI and their corresponding textual reports. Moreover, learning

joint representations across modalities typically requires large, labeled datasets, which are often unavailable in clinical settings. This problem in cross-modal learning is graphically illustrated in Figure 1a

2.2. PIRTA: Paired Image-domain Retrieval and Text-domain Augmentation

To overcome the challenges of cross-modal learning, we propose PIRTA, which reformulates the cross-modal learning problem as an in-domain retrieval task, thereby reducing the complexity. Instead of learning a text encoder $f_{\text{text}} : \mathcal{Y} \rightarrow \mathcal{Z}$, we focus solely on training an image encoder $f_{\text{image}} : \mathcal{X} \rightarrow \mathcal{Z}$, and leverage a paired image-text database with m samples:

$$\mathcal{D} = \{(x_i, y_i)\}_{i=1}^m, \quad (6)$$

where each image $x_i \in \mathcal{X}$ is associated with a corresponding ground-truth radiology report $y_i \in \mathcal{Y}$.

The key idea is to minimize the distance between the query image x_q and a similar image x_i from the database \mathcal{D} , where the similarity is measured in the shared latent space \mathcal{Z} . Formally, the goal is now to find the image x_i that minimizes the following distance:

$$d(f_{\text{image}}(x_q), f_{\text{image}}(x_i)). \quad (7)$$

Once the most similar image x_i is retrieved, its paired radiology report y_i is used to augment the report generation process for x_q , ensuring that the generated report remains clinically relevant and factual. By casting the problem as a retrieval task, PIRTA reduces the hypothesis space to $\mathcal{H}_{\text{image}}$, effectively lowering the overall complexity:

$$C(\mathcal{H}_{\text{PIRTA}}) = C(\mathcal{H}_{\text{image}}). \quad (8)$$

Given that $C(\mathcal{H}_{\text{image}}) \geq 0$, it is trivial that

$$C(\mathcal{H}_{\text{image}}) + C(\mathcal{H}_{\text{text}}) \geq C(\mathcal{H}_{\text{PIRTA}}), \quad (9)$$

showing that the PIRTA framework simplifies the learning task, making it more feasible in practice, especially in clinical settings where data is scarce.

The reduction in complexity from cross-modal learning to single-modality retrieval can be understood more rigorously in terms of the data distributions involved. In the original cross-modal learning setting, the model must approximate the joint distribution $P(x, y)$, which involves learning both $P(y|x)$ and $P(x|y)$. This is a significantly harder problem due to the need for joint alignment between the modalities.

In contrast, PIRTA focuses on learning only the marginal distribution $P(x)$, which is a much simpler task. Given that the paired database \mathcal{D} contains high-quality radiology reports y_i corresponding to the retrieved images x_i , PIRTA avoids the need to model the conditional distributions entirely. The retrieval of relevant text information from the paired database ensures factual accuracy, while the image encoder learns meaningful representations in a lower-complexity space.

Thus, the complexity of PIRTA’s retrieval task is constrained by the data distribution over the image space, $P(x)$, rather than the joint distribution $P(x, y)$. This reduction in the complexity of the hypothesis space, along with the focus on retrieval, makes PIRTA a highly efficient and scalable framework for radiology report generation.

Once the most similar image x_i is retrieved based on minimizing $d(f_{\text{image}}(x_q), f_{\text{image}}(x_i))$, the paired radiology report y_i from the database is used to augment the final report generation process. This augmentation step improves the factuality of the generated report, as it is grounded in real, clinically verified reports associated with the retrieved images.

The PIRTA framework thereby bypasses the need to explicitly align image and text representations in the latent space, leveraging retrieval to improve the factual accuracy of the generated reports. This also reduces the reliance on large-scale labeled datasets, as the retrieval-based augmentation relies on the existence of a pre-built paired image-text database. This solution to cross-modal learning with PIRTA is graphically illustrated in Figure 1b

2.3. Experiments

2.3.1. Datasets

From March 2016 to June 2022, a total of 1,831 patients (993 with acute stroke and 838 without), aged 18 years or older, who underwent brain MRI for previously diagnosed or suspected stroke, were retrospectively

Table 1: Examples of the raw radiology report and the structured radiological findings.

	Raw radiology reports	Structured radiological findings
Example #1	Diffusion restriction involving Lt. superior frontal and Lt. precentral gyrus. Tiny diffusion restricted lesion in Lt. middle frontal gyrus - with T2 hyperintense change → Acute infarction	There is [mild] [large vascular territorial] diffusion restriction in the [anterior circulation] territory.
Example #2	Diffusion restriction lesions in right inferior cerebellum - no definite T2 hyperintense change - r/o hyperacute infarctions	There is [strong] [small] diffusion restriction in the [posterior circulation] territory.
Example #3	Diffusion restriction in left basal ganglia. - T2 high SI, no hemorrhage. → R/O Acute infarction	There is [mild] [small lacune] diffusion restriction in the [deep gray matter] territory.

enrolled from three institutions: Seoul National University Hospital (SNUH) (n=818), Seoul Metropolitan Government-Seoul National University Boramae Medical Center (BRMH) (n=580), and Seoul National University Bundang Hospital (SNUBH) (n=227). The stroke MRI protocol required, at a minimum, the acquisition of fluid-attenuated inversion recovery (FLAIR) and DWI sequences. The dataset, which includes cases from two tertiary care facilities, comprises multi-vendor MRI cases with high variability in stroke lesion size, quantity, and location. The DWI sequence included a trace image with a b-value up to 1000 s/mm² and a corresponding ADC map. Imaging was performed using various MRI systems as part of the routine clinical protocol for stroke patients, including 3T Philips MRI scanners (Achieva, Ingenia, Ingenia CX), 3T Siemens MAGNETOM MRI scanners (Skyra, Skyra Fit), 3T GE MRI scanners (Premier, Discovery 750W), 1.5T Philips MRI scanners (Ingenia, Achieva, Intera), and 1.5T Siemens MAGNETOM MRI scanners (Amira). Raw radiology reports paired with the MRI data were also collected for all enrolled subjects. The study received approval from the Institutional Review Boards of all participating institutions, with a waiver for informed consent (No. 2303-157-1417).

Several preprocessing steps were applied to the MRI images. Initially, skull stripping was carried out using SynthSeg on all brain MRI modalities to eliminate non-brain tissues. Following this, to optimize memory usage and standardize the resolution across different datasets, the images were downsampled and padded to a voxel size of 96 x 112 x 48 along the (x, y, z) axes, with a resolution of (2, 2, 4). Lastly, N4 Bias Field Correction was applied to address distortions caused by bias fields from varying scanners, ensuring uniform signal intensity across the im-

ages.

Raw radiology reports were also preprocessed into formatted radiological findings for fine-tuning the LLM. Specifically, the raw radiology reports were rephrased based on a template sentence for radiological findings that included different 1) classes, 2) infarction types, and 3) ischemic territory information. Classes were categorized as strong or mild; infarction types were classified into large vascular territorial, wedge-shaped vascular territorial, small lacune, small striato-capsular, and small diffusion restriction; ischemic territories were divided into three specific regions: posterior circulation, anterior circulation, and deep gray matter. The preprocessing of the raw radiology report into structured findings was done by a board-certified neuroradiologist with over 5 years of experience. Examples of the raw radiology report and the preprocessed radiological findings are provided in Table 1.

Public datasets that include brain imaging data were further collected for pretraining and external validation. Specifically, unlabeled DWI and ADC images from a total of 38,532 subjects were obtained from the UK Biobank (Alfaro-Almagro et al., 2018) for pretraining the image encoder and labeled imaging data from the Ischemic Stroke Lesion Segmentation (ISLES) 2022 challenge from 211 subjects for externally validating the proposed method (Hernandez Petzsche et al., 2022). The in-house datasets from SNUH and SNUBH are merged and used for training the image encoder, thus indicated as the *internal* set, while the datasets from BRMH and ISLES are solely used for testing the performance, thus indicated as the *external* set. The full description of the dataset used in this study is summarized in Table 2.

Table 2: Distribution of the datasets used in this study.

	Organization	Total	Normal	Stroke territory		
				Anterior	Deep gray	Posterior
Pretrain set	UK Biobank	38,532		N/A		
Train set (internal)	SNUH	648	413	110	66	59
	SNUBH	179	0	123	38	18
Test set (internal)	SNUH	170	102	30	20	18
	SNUBH	48	0	29	14	5
Test set (external)	BRMH	580	323	100	78	79
	ISLES	206	0	77	52	77

2.3.2. Implementation details

The training process for the image encoder is conducted in two stages: the SSL and the supervised fine-tuning (SFT). In the first stage, MAE-based SSL was performed with both DWI and ADC images. The two MRI sequences are concatenated along the channel dimension to form a 2-channel 3D volume. This volume is then divided into smaller volume patches, flattened to serve as input vectors. Positional embeddings are added to provide location information, and a random mask is applied to remove $(1-q)$ of the patches. The remaining patches are input to the image encoder to learn dense representations. Subsequently, a lightweight image decoder reconstructs the masked volume patches. The ViT architectures are used for both the image encoder and the decoder. Training is performed with the AdamW optimizer to minimize mean squared error (MSE), with a mask ratio q of 0.25, a learning rate of 6.4×10^{-3} , and a weight decay of 0.05, over 500 epochs. To validate the scaling effect with respect to the dataset size, we define the *small dataset*, and the *large dataset* for pretraining as the dataset that includes only the SNUH+SNUBH internal training set ($n=827$), and that additionally includes the UKB dataset ($n=39,259$), respectively.

In the second stage, the image encoder is fine-tuned to classify the stroke lesion into one of the four classes, i.e. anterior, deep gray, posterior, and normal. The ViT encoder remains unchanged, whereas the reconstruction decoder is replaced with a linear layer for the classification task. The training set from SNUH and SNUBH was used for the SFT in this stage. The AdamW optimizer is utilized to minimize cross-entropy loss. We employ a learning rate of 1×10^{-3} and a weight decay of 0.05, and the model is trained for 1000 epochs. Schematic illustration of training the image encoder is presented in Figure 2a.

After the training of the image encoder, the most rele-

vant images can be retrieved based on the latent vectors of the representation space. In specific, we first construct a pre-defined image database, \mathcal{D} , using the representation features extracted from the fine-tuned ViT for MRI images in the training set. Then, the representation feature of the query MRI image is obtained. The cosine similarity

Table 3: An exemplar instruction data for fine-tuning the LLM. Training the LLM is done with the structured radiology report format data as given in the 'Input' box, with expected generation output to follow the structure of the data given in the 'Generated' box. Ground-truth labels, highlighted in blue, are included during training and suppressed during inference.

Input
<pre> <s> [INST] Provide proper clinical report based on Registry and Similar patient reports. ### Registry: 75-year-old, Female, Altered Mentality, 32.0, HTN, Afib, ### Similar patient reports: [1] [#Top-1 image-domain retrieval case's radiological finding] [2] [#Top-2 image-domain retrieval case's radiological finding] [3] [#Top-3 image-domain retrieval case's radiological finding] [4] [#Top-4 image-domain retrieval case's radiological finding] [5] [#Top-5 image-domain retrieval case's radiological finding] [/INST] Clinical Presentation: A 75-year-old Female patient with Altered Mentality. NIHSS: 32.0 Past Medical History: HTN, Afib Findings: There is a diffusion restriction in the anterior circulation territory. Impression: Acute infarction </pre>
Generated
<pre> Clinical Presentation: A 75-year-old Female patient with Altered Mentality. NIHSS: 32.0. Past Medical History: HTN, Afib, Findings: There is a diffusion restriction in the anterior circulation territory Impression: Acute infarction ### Similar patient reports: [1] Similarity Score : 0.87 There is mild wedge-shaped vascular territorial diffusion restriction in the anterior circulation territory. [2] Similarity Score : 0.86 There is mild wedge-shaped vascular territorial diffusion restriction in the anterior circulation territory. [3] Similarity Score : 0.86 There is mild large vascular territorial diffusion restriction in the anterior circulation territory. [4] Similarity Score : 0.86 There is mild large vascular territorial diffusion restriction in the anterior circulation territory. [5] Similarity Score : 0.86 There is mild wedge-shaped vascular territorial diffusion restriction in the anterior circulation territory. </pre>

is calculated as the distance, d , between this query feature and the embedding features stored in the database \mathcal{D} . The images with the greatest cosine similarity are retrieved and considered the most relevant.

For generating the radiology reports, an LLM was trained to generate radiology reports based on the structured radiological findings of the retrieved images. Specifically, instruction fine-tuning of LLaMA3-8B-Instruct¹ was conducted using the low-rank adaptation (LoRA) (Hu et al., 2021). The LoRA fine-tuning of LLaMA-3 was optimized over 10 epochs with a batch size of 16, and the hyper-parameter number of samples m was set to 5. The final radiology report provides 5 types of information: clinical presentation, NIH Stroke Scale (NIHSS), past medical history, findings, and the final impression. Schematic illustration of the radiology report generation with PIRTA is presented in Figure 2b.

The clinical presentation, NIHSS, and past medical history are given to the LLM as part of the instruction when generating the report. Additionally, the top 5 radiology findings retrieved with the image encoder are appended at the bottom of the radiology report along with the similarity score so that clinicians can refer to the original data that augmented the generation process. An exemplar data structure of the input and generated part of the LLM is provided in Table 3.

All experiments were performed on a Linux server with 4 NVIDIA A6000 GPUs.

2.3.3. Evaluation metrics

The performance of the image encoder for the retrieval task was evaluated using mean average precision (mAP) and top-k accuracy (Acc@k). Precision is defined as the ratio of relevant images among the retrieved images:

$$\text{Precision} = \frac{(\# \text{ of relevant items in retrieved items})}{(\# \text{ of retrieved items})}.$$

Average precision (AP@n) is calculated as follows:

$$\text{AP@n} = \frac{1}{N} \sum_{k=1}^n \text{P@k} \times \text{rel@k},$$

where N represents the total number of relevant items, P@k is the precision at rank k , and rel@k is 1 if the im-

age at rank k is relevant. The maximum rank considered is denoted by n . mAP@n score is then computed as:

$$\text{mAP@n} = \frac{1}{Q} \sum_{i=1}^Q \text{AP@n}_i,$$

where Q represents the number of query images. Thus, mAP provides the average AP across all queries.

Acc@k measures whether the correct answer appears among the top k retrieved results. It is calculated using:

$$\text{Acc@k} = \frac{1}{N} \sum_{i=1}^N \sum_{j=1}^k 1(\hat{y}_{i,j} = y_{i,j}),$$

where N is the total number of queries, and $1(\hat{y}_{i,j} = y_{i,j})$ equals 1 if the correct answer is within the top k predictions for query i , and 0 otherwise. Acc@k represents the average of these binary outcomes, indicating whether the correct answer is included in the top k predictions.

To further evaluate the performance of text-domain augmentation, we conducted a quantitative evaluation of the Acc@1 of ischemic territory information extracted from the generated reports, comparing these results with those obtained from image-domain retrieval.

3. Results

3.1. Quantitative evaluation

3.1.1. MRI Image retrieval

Table 4: Quantitative image retrieval performance with respect to the size of the pretraining dataset.

Evaluation dataset	Pretrain	mAP@1	mAP@5	mAP@10	Acc@1	Acc@5	Acc@10
SNUH+SNUBH (internal)	No	80.73	81.9	81.57	80.73	84.4	84.4
	Small	90.37	90.78	90.85	90.37	91.74	92.66
	Large	94.04	94.27	94.15	94.04	94.5	94.5
BRMH (external)	No	56.72	58.22	57.94	56.72	61.55	64.48
	Small	68.97	69.19	69.11	68.97	70.17	70.69
	Large	71.21	71.43	71.3	71.21	71.72	71.72
ISLES (external)	No	38.83	40.48	40.42	38.83	44.17	48.06
	Small	65.53	66.26	66.39	65.53	67.48	69.42
	Large	70.87	71.52	71.24	70.87	72.33	72.82

The retrieval of relevant MRI images was quantitatively evaluated to assess the performance of the proposed PIRTA framework, particularly in the context of retrieving the most relevant images for paired text augmentation. Three key metrics were used: mean average precision (mAP), top-k accuracy (Acc@k), and precision.

¹<https://huggingface.co/meta-llama/Meta-Llama-3-8B-Instruct>

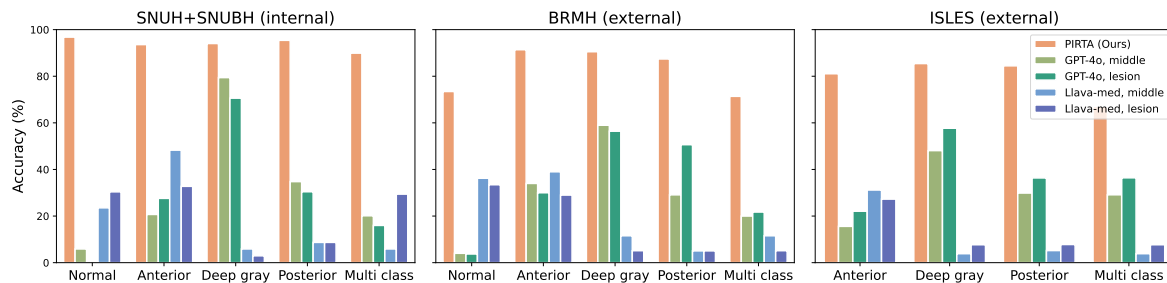


Figure 3: Quantitative performance of the proposed method compared to baseline. SNUH+SNUBH are internal datasets, in which the separate train set data from the same institutions were used for SFT, while BRMH and ISLES are external datasets.

As shown in Table 4, the image encoder pretrained using the masked autoencoder (MAE) framework outperformed non-pretrained encoders, achieving higher mAP and Acc@k values. The large-scale dataset from the UK Biobank, consisting of over 38,000 subjects, enabled the best performance, highlighting the benefit of using extensive pretraining data.

When applied to the internal dataset (SNUH+SNUBH), the model achieved a mAP@1 of 94.04%, a significant improvement compared to the non-pretrained model’s 80.73%. Similar improvements were observed for external datasets, including the BRMH and ISLES sets, where the pretrained model on large data achieved 71.21% and 70.87%, respectively, in mAP@1.

These results underscore the importance of pretraining, particularly on large datasets, to learn high-quality image representations. The PIRTA framework was effective in retrieving 3D DWI images that were relevant not only within the training domain but also across external test sets, demonstrating its potential for generalization in clinical environments with varying data distributions.

3.1.2. Radiology report generation

For the radiology report generation task, the PIRTA framework was compared to GPT-4o, a state-of-the-art large language model (LLM) known for its capabilities in image-to-text generation, and LLaVA-Med (Li et al., 2024), which is a VLM trained with large-scale medical image data. The accuracy of ischemic territory detection was used as the primary evaluation metric, as this information is critical for diagnosing and planning treatments in stroke patients.

Since GPT-4o and LLaVA-Med can only handle 2D images, we provided the model with a 2D axial slice image selected from either the middle of the brain or from the center of the stroke lesion. Given the 2D axial slice image, the baseline models were instructed to directly generate the radiology report, providing one example of the desired structured report format. While the both GPT-4o and LLaVA-Med struggled to generate accurate reports from the input DWI image slice, the proposed PIRTA reached a significantly higher Acc@1 for ischemic territory detection across the internal and external datasets, compared to the baseline models as can be see in Figure 3.

The enhanced performance can be attributed to PIRTA’s ability to retrieve clinically relevant images and use paired text-domain information to improve the quality of the generated reports. These results indicate the superiority of PIRTA in clinical report generation tasks that require understanding complex 3D volumetric data.

3.2. Qualitative evaluation

3.2.1. MRI image retrieval

Qualitative examples of MRI image retrieval highlight the effectiveness of PIRTA in distinguishing between different ischemic territories. Figure 4 showcases retrieval results for anterior, deep gray, and posterior ischemic territories, with the majority of retrieved images being accurate, especially for the image encoder pretrained with the large dataset. Correct retrieval results are marked with green borders, demonstrating PIRTA’s ability to capture subtle differences in the ischemic territories.

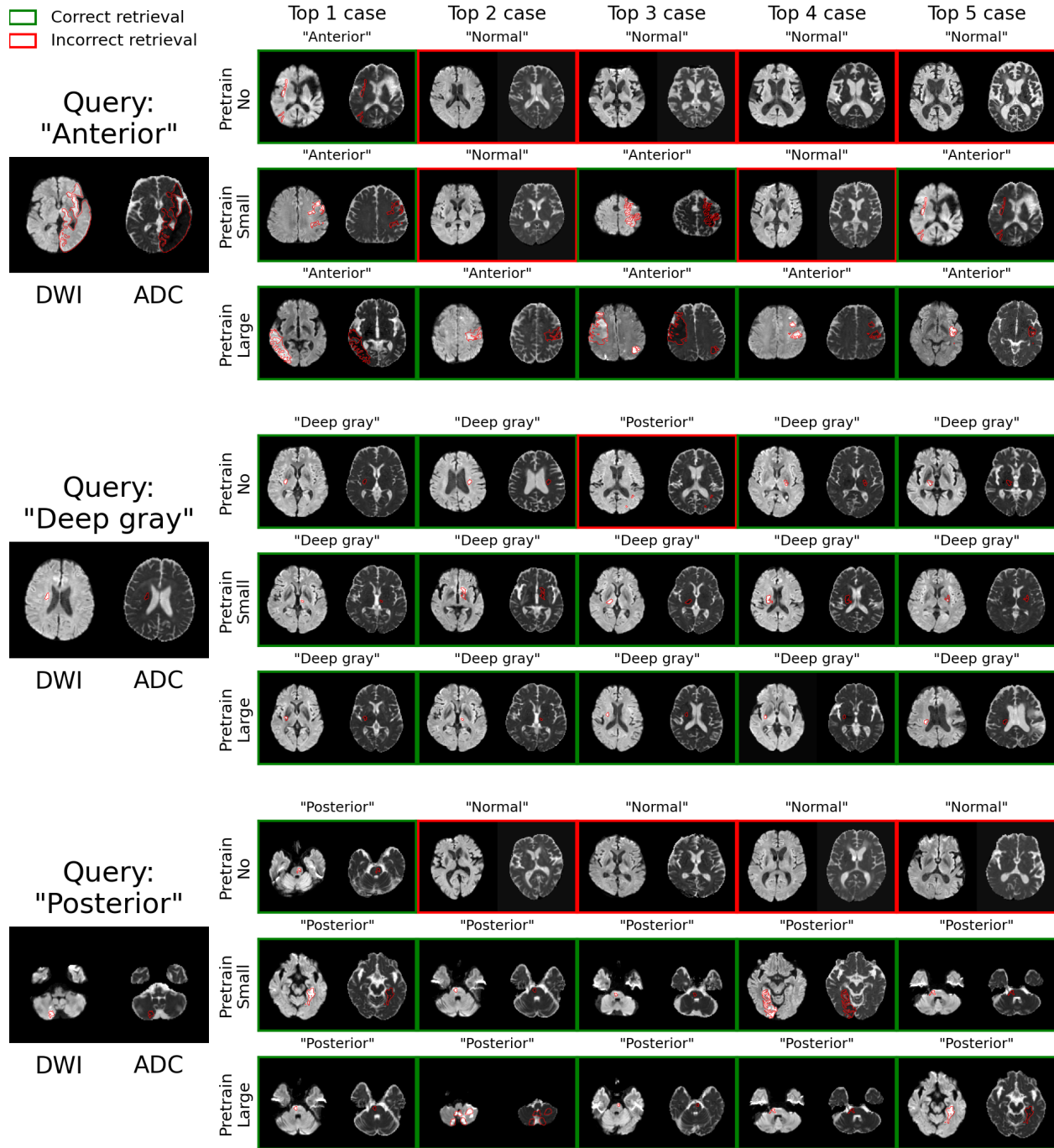
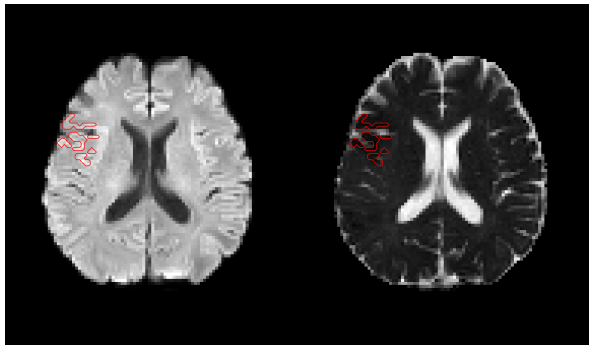
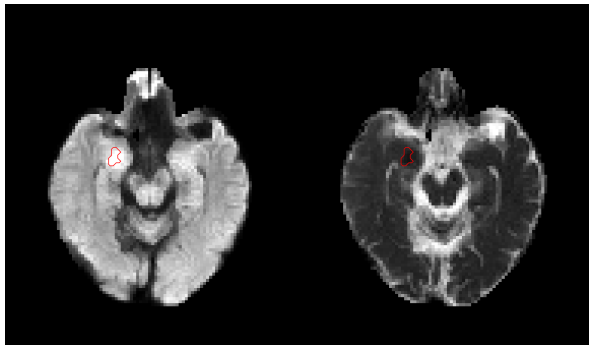


Figure 4: Retrieval results on three classes. five scans are retrieved for each query. The first column displays the query image, while the following columns present the retrieved scans for each query, arranged in rank order. A red contour in MRI scans signifies a stroke infarction lesion. False retrieval is indicated by a red bounding box, while True retrieval is indicated by a green bounding box. "No" indicates pretraining, "Small" indicates pretraining with the small dataset, and "Large" indicates pretraining with the large dataset.

Table 5: A qualitative assessment of text-domain augmentation is provided. Correct generation of the ischemic territory information with corresponding similarity scores are highlighted in **blue** font, while incorrect ones are highlighted in **red** font.

First Example	Second Example
Input image	Input image
	
Ground-truth label	Ground-truth label
<p>Clinical Presentation: A 58-year-old Male patient. NIHSS: N/A Past Medical History: Findings: There is a diffusion restriction in the anterior circulation territory. Impression: Acute infarction</p>	<p>Clinical Presentation: A 71-year-old Male patient with Altered Mentality. NIHSS: 24.0 Past Medical History: HTN, Afib Findings: There is a diffusion restriction in the anterior circulation territory. Impression: Acute infarction</p>
Generated	Generated
<p>Clinical Presentation: A 58-year-old Male patient. NIHSS: N/A. Past Medical History: Findings: There is a diffusion restriction in the anterior circulation territory. Impression: Acute infarction ### Similar patient reports: [1] Similarity Score: 0.95 There is mild wedge-shaped vascular territorial diffusion restriction in the anterior circulation territory. [2] Similarity Score: 0.93 There is mild small striatocapsular diffusion restriction in the anterior circulation territory. [3] Similarity Score: 0.91 There is mild large vascular territorial diffusion restriction in the anterior circulation territory. [4] Similarity Score: 0.91 There is mild large vascular territorial diffusion restriction in the anterior circulation territory. [5] Similarity Score: 0.90 There is strong small diffusion restriction in the anterior circulation territory.</p>	<p>Clinical Presentation: A 71-year-old Male patient with Altered Mentality. NIHSS: 24.0 Past Medical History: HTN, Afib Findings: There is a diffusion restriction in the deep gray matter territory. Impression: Acute infarction ### Similar patient reports: [1] Similarity Score: 0.53 There is mild small lacune diffusion restriction in the deep gray matter territory. [2] Similarity Score: 0.52 There is mild small striatocapsular diffusion restriction in the deep gray matter territory. [3] Similarity Score: 0.49 There is strong small diffusion restriction in the deep gray matter territory. [4] Similarity Score: 0.48 There is mild small striatocapsular diffusion restriction in the deep gray matter territory. [5] Similarity Score: 0.46 There is mild small striatocapsular diffusion restriction in the deep gray matter territory.</p>

Incorrect retrievals, marked in red, tended to occur when there were overlapping features between territories, such as small infarcts that span multiple regions. However, these errors were rare, particularly in the model pre-trained with the large dataset, which consistently retrieved highly relevant images. The visual analysis of retrievals illustrates that PIRTA can generalize well across different stroke lesion locations and imaging artifacts.

3.2.2. Radiology report generation

Qualitative assessments of radiology report generation demonstrate PIRTA’s capacity to generate clinically useful reports that align with expert-written reports. As seen in Table 5, PIRTA’s augmented reports include critical details such as ischemic territory, clinical presentation, and NIHSS scores, with similarity scores provided for the retrieved images. Specifically, the first example showed definite cortical diffusion restriction in the right frontal operculum and insula on DWI/ADC images. The lesions were located within the right middle cerebral artery territory, categorized as an anterior circulation. The generated report correctly described the stage as acute, and vascular territory as anterior circulation. The second example was the difficult case with isolated amygdala infarction. The generated report correctly described the stage as acute, but incorrectly described territorial classification as deep gray matter, while the ground truth was anterior circulation (Table 5). In summary, reports generated by PIRTA were particularly strong in identifying the ischemic territory and type of diffusion restriction, achieving high accuracy when the similarity scores between the query and retrieved images were high. This suggests that the RAG process of PIRTA directly improves report factuality, especially when the retrieval step is accurate.

For comparison, we conducted a qualitative analysis of the task of identifying ischemic territory using GPT-4o and LLaVA-Med. When two models were asked to generate the final output in the format of *There is a diffusion restriction in the anterior/posterior/deep gray circulation territory.*, GPT-4o generated outputs that adhered to the given format, whereas LLaVA-Med rarely followed the format precisely. Instead, LLaVA-Med tended to generate similar sentences with additional explanations or only included label information. In most cases, LLaVA-Med did not complete the task but rather repeated the prompt or provided conceptual explanations about MRI images.

Table 6: Classification performance and the effect of dataset scaling in pretraining the image encoder

Dataset	Pretrain	Class wise Acc@1				Multi class Acc@1
		Normal	Anterior	Deep gray	Posterior	
SNUH+SNUBH (internal)	No	96.3	87.96	89.81	89.81	81.94
	Small data	99.54	93.06	91.67	95.37	89.81
	Large data	100.0	95.37	93.98	96.76	93.06
BRMH (external)	No	60.87	78.26	86.29	83.95	53.18
	Small data	69.23	89.8	90.47	85.95	66.22
	Large data	72.24	90.64	90.8	87.79	69.23
ISLES (external)	No	-	69.52	76.67	68.1	40.0
	Small data	-	84.29	86.67	80.95	61.9
	Large data	-	82.38	84.76	83.81	68.1

3.3. Further experiments

3.3.1. Learned representation quality study

We evaluated the performance of the classification downstream task, as shown in Table 6. The image encoder pretrained on a large dataset not only excelled in retrieval tasks but also exhibited high accuracy in classification. The model pretrained on extensive data significantly enhanced multi-class classification performance, achieving substantial improvements on both the internal test set and two external test sets. Furthermore, it attained the highest class-wise accuracy for most categories. This outstanding performance underscores the model’s capacity to extract more generalized and diverse features through pre-training, thereby boosting its ability to accurately identify stroke lesions.

Through the representation learning obtained from pre-training and fine-tuning, the image encoder forms a conceptual space for predicting stroke lesions. Figure 5 illustrates this by projecting the 768-dimensional features into a 2D manifold using UMAP, which preserves both the local and global structure of the high-dimensional space. Each stroke lesion is color-coded according to its type. A qualitative evaluation reveals that the image encoder without pretraining shows overlapping spaces for normal, deep gray, and posterior regions. While even the encoder pretrained with the small dataset exhibits some overlap between normal and posterior spaces, the model pretrained on the large dataset clearly distinguishes the feature spaces corresponding to each lesion type. Moreover, when clustering with a Gaussian Mixture Model, the highest Silhouette Score—a metric used to assess the quality of clustering—was observed for the large dataset pretrained image encoder, indicating superior clustering performance in the representation space.

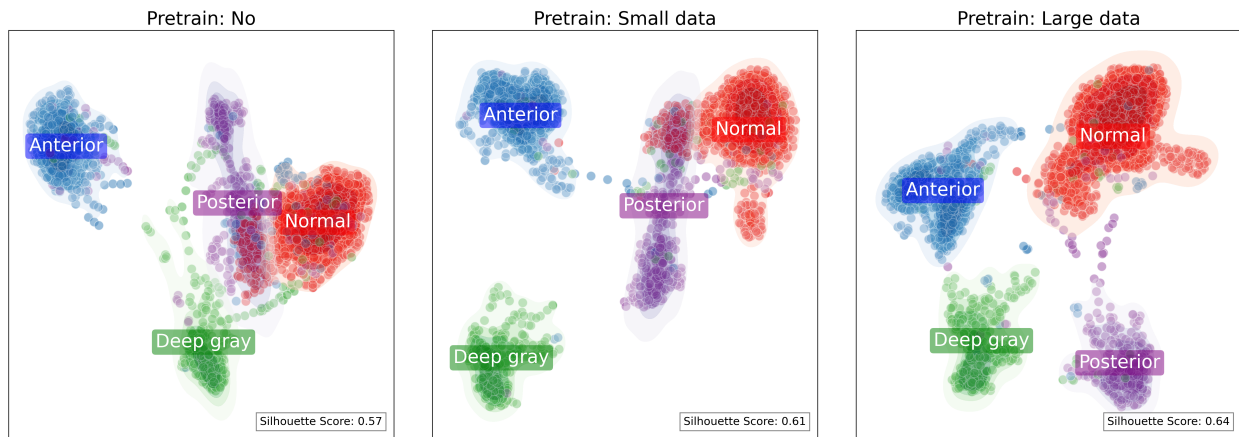


Figure 5: The 768-dimensional feature vectors derived image encoder are projected into a 2D manifold using UMAP. Each stroke lesion type is color-coded. "No" indicates no pretraining, "Small" indicates pretraining with the small dataset, and "Large" indicates pretraining with the large dataset.

4. Discussion

The proposed PIRTA framework presents an advancement in the automated generation of radiology reports from 3D MRI data by improving the accuracy and factuality of these reports, addressing the key challenges in cross-modal translation from 3D imaging data to clinically useful textual reports.

Given that 75% of stroke-related deaths now occur in developing countries, largely due to population aging (Feigin et al., 2015), PIRTA’s application in hospitals with limited access to on-site neurologists or neuroradiologists could significantly support timely clinical decisions, particularly for emergency thrombolytic interventions during critical off-hours. In such settings, PIRTA’s automated reporting can help prevent diagnostic delays that might otherwise narrow the therapeutic window essential for acute ischemic stroke management (Powers et al., 2019), ultimately improving outcomes in regions facing a disproportionate stroke burden. Additionally, by reducing reading times with preliminary automated reports, PIRTA can ease radiologists’ workload and offer critical support even in developed countries facing high patient volumes and time constraints (Hosny et al., 2018; McDonald et al., 2015).

One of the main challenges in medical imaging analysis is aligning 3D imaging data with radiologic reports,

which also slightly differ in data distribution from natural language descriptions. Current cross-modality alignment approaches, including recent multimodal approaches such as LLaVA-Med (Li et al., 2024) and GPT-4o, often face limitations due to inherent modality gaps, which hinder the accuracy and effectiveness of alignment (Huo et al., 2024; Ma et al., 2024). Traditional techniques typically rely on deep learning models to directly map between image and text domains, requiring extensive labeled datasets and parallel training of image and text encoders. This approach not only escalates computational complexity but also poses difficulties in learning coherent representations across such distinct data types. PIRTA addresses these challenges by reimagining cross-modality alignment as an in-domain retrieval problem, followed by text-domain augmentation. Rather than building cross-modal mappings from scratch, PIRTA employs a simple retrieval-augmented generation strategy that matches a query image with similar images from a database, each paired with clinically verified text reports. This approach simplifies the alignment process and effectively bridges modality gaps, resulting in improved accuracy and factuality in radiologic report generation.

In evaluating PIRTA’s performance, it is important to highlight how it compares to existing models. While GPT-4o has shown strong performance in generating natural language descriptions from 2D images, its application to

3D medical data has been limited. This is primarily due to the lack of pretrained 3D encoders and the challenges in handling volumetric data. GPT-4o, for instance, was tested on 2D axial slices selected from the middle of the brain or from the center of the stroke lesion, yet it consistently underperformed when compared to PIRTA in both accuracy and relevance of the generated reports. PIRTA’s ability to handle full 3D volumes and retrieve relevant, clinically verified reports gives it a distinct advantage, especially in complex cases like stroke diagnosis. This limitation of leveraging 3D images was also evident in the case of LLaVA-Med (Li et al., 2024), which is a VLM specialized for medical images.

Additionally, PIRTA’s image encoder, pretrained MAE on large-scale, unlabeled 3D MRI datasets, demonstrated superior performance in both retrieval and classification tasks. The quantitative results show that PIRTA achieved a high mAP and accuracy across different top-k settings, significantly outperforming models that did not use pretraining. Pretraining with a large dataset further improved performance, suggesting that the model’s ability to generalize across different types of stroke lesions and imaging variations is greatly enhanced through the pretraining process.

The size and quality of the pretraining dataset play a pivotal role in PIRTA’s success. As shown in the experiments, the image encoder pretrained on the large dataset of over 38,000 subjects from the UK Biobank significantly outperformed models trained on smaller datasets or without pretraining. This indicates that pretraining on a diverse and large-scale dataset is crucial for learning robust image representations (Ke et al., 2021), particularly for complex tasks such as stroke lesion identification. The results also demonstrate that using larger datasets for pretraining leads to higher accuracy not only in image retrieval tasks but also in downstream classification tasks, where the model correctly classified stroke subtypes with high precision.

Moreover, the benefits of pretraining extend to the external validation datasets as well, where PIRTA continued to show robust performance even when tested on datasets from different institutions and with different scanner vendors. This highlights the model’s ability to generalize across different imaging environments, a critical factor for any AI system that is to be deployed in real-world clinical settings.

Automated report generation systems have the potential to alleviate the burden on radiologists, particularly in high-pressure environments like stroke units, where “time is brain”, or timely diagnosis is critical. By providing accurate and clinically relevant reports, PIRTA can assist clinicians in making more informed decisions, potentially reducing the time to diagnosis and improving patient outcomes. Delayed diagnosis can miss the narrow therapeutic window of acute ischemic stroke and delayed injection of thrombolytic agents can lead to increased symptomatic hemorrhagic change (The National Institute of Neurological Disorders and Stroke rt-PA Stroke Study Group, 1995; Xiong et al., 2024).

In a qualitative assessment of the incorrect case (Table 5), the model struggled with an isolated acute infarction in the amygdala, a rare site for ischemic changes (Alves et al., 2022; Beh et al., 2016) that may have complicated image embedding retrieval, resulting in lower top-5 similarity scores. The report incorrectly identified the lesion as deep gray matter (i.e., basal ganglia), likely due to the anatomical proximity of the amygdala. This location typically suggests small vessel disease rather than large artery disease (Wardlaw et al., 2019). In summary, variable arterial supply and susceptibility to false-positive diffusion signals from artifacts add complexity to accurate lesion classification. This interesting result suggests the need for a prospective multi-reader clinical study, where neuroradiologists qualitatively assess PIRTA’s performance to better understand its clinical value.

However, there are several areas where PIRTA can be further improved. One limitation of the current study is its reliance on DWI and ADC images. While these modalities are critical for stroke diagnosis, incorporating additional imaging modalities, such as PWI or T2-weighted imaging, could provide a more comprehensive view of the patient’s condition. Future work could explore the integration of these modalities into PIRTA’s framework, potentially improving the quality and depth of the generated reports.

Another avenue for improvement is the inclusion of more diverse clinical data. In the current implementation, PIRTA generates reports based on imaging data alone, with some augmentation from patient history and presentation. Integrating other clinical data sources, such as real-time lab results or genetic information, could enhance the factuality and relevance of the generated reports. This

would require the model to handle multi-modal data beyond imaging and text, but it could significantly increase the utility of the system in clinical decision-making.

Additionally, while PIRTA performs well in stroke diagnosis, its generalizability to other medical domains remains to be fully explored. Future studies could investigate the application of PIRTA to other types of medical imaging, such as cancer detection in CT or MRI, or even pathology in digital slides. Given the generalizability of the retrieval-augmented generation approach, PIRTA could potentially be adapted to a wide range of medical applications where factuality and accuracy are paramount.

While PIRTA represents a significant improvement over existing methods, several challenges remain. One limitation is the reliance on high-quality, labeled datasets for pretraining and fine-tuning. Although SSL methods like MAE have reduced the dependence on labeled data, there is still a need for large, curated datasets to achieve optimal performance. The scarcity of such datasets in clinical settings remains a bottleneck, particularly in specialized domains like neurology or oncology.

Moreover, PIRTA's performance in cases with lower similarity scores between the query image and retrieved images highlights the need for further refinement of the retrieval process. One possible direction for future work is to explore more advanced retrieval mechanisms that can handle cases with lower similarity more effectively, such as hybrid retrieval approaches that incorporate both image features and contextual clinical information.

5. Conclusion

We propose PIRTA, a cross-modal RAG framework for generating radiology reports from 3D medical images with improved factuality. PIRTA mitigates the need for learning cross-modal mapping by casting the problem as an in-domain retrieval of similar images that have paired ground-truth radiology reports. Experimental results demonstrate that PIRTA outperforms state-of-the-art multimodal language models in generating clinically accurate AIS radiology reports from 3D DWI images.

References

Alfaro-Almagro, F., Jenkinson, M., Bangerter, N.K., Andersson, J.L., Griffanti, L., Douaud, G., Sotiropoulos,

S.N., Jbabdi, S., Hernandez-Fernandez, M., Vallee, E., et al., 2018. Image processing and quality control for the first 10,000 brain imaging datasets from uk biobank. *Neuroimage* 166, 400–424.

Alves, I.S., Coutinho, A.M.N., Vieira, A.P.F., Rocha, B.P., Passos, U.L., Gonçalves, V.T., Silva, P.D.S., Zhan, M.X., Pinho, P.C., Delgado, D.S., Docema, M.F.L., Lee, H.W., Policeni, B.A., Leite, C.C., Martin, M.G.M., Amancio, C.T., 2022. Imaging aspects of the hippocampus. *Radiographics* 42, 822–840.

Beh, S.M.J., Cook, M.J., D'Souza, W.J., 2016. Isolated amygdala enlargement in temporal lobe epilepsy: A systematic review. *Epilepsy Behav.* 60, 33–41.

Bommasani, R., Hudson, D.A., Adeli, E., Altman, R., Arora, S., von Arx, S., Bernstein, M.S., Bohg, J., Bosselut, A., Brunskill, E., et al., 2021. On the opportunities and risks of foundation models. *arXiv preprint arXiv:2108.07258* .

Borgeaud, S., Mensch, A., Hoffmann, J., Cai, T., Rutherford, E., Millican, K., ..., Irving, G., 2022. Improving language models by retrieving from trillions of tokens, in: *Proceedings of the 39th International Conference on Machine Learning (ICML)*, PMLR. pp. 2206–2219.

Campbell, B.C., De Silva, D.A., Macleod, M.R., Coutts, S.B., Schwamm, L.H., Davis, S.M., Donnan, G.A., 2019. Ischaemic stroke. *Nature reviews Disease primers* 5, 70.

Caron, M., Touvron, H., Misra, I., Jégou, H., Mairal, J., Bojanowski, P., Joulin, A., 2021. Emerging properties in self-supervised vision transformers, in: *Proceedings of the IEEE/CVF international conference on computer vision*, pp. 9650–9660.

Cetinoglu, Y.K., Koska, I.O., Uluc, M.E., Gelal, M.F., 2021. Detection and vascular territorial classification of stroke on diffusion-weighted mri by deep learning. *European Journal of Radiology* 145, 110050.

Dosovitskiy, A., Beyer, L., Kolesnikov, A., Weissenborn, D., Zhai, X., Unterthiner, T., Dehghani, M., Minderer, M., Heigold, G., Gelly, S., et al., 2020. An image is worth 16x16 words: Transformers for image recognition at scale. *arXiv preprint arXiv:2010.11929* .

- Feigin, V.L., Brainin, M., Norrving, B., Martins, S., Sacco, R.L., Hacke, W., Fisher, M., Pandian, J., Lindsay, P., 2022. World stroke organization (wso): global stroke fact sheet 2022. *International Journal of Stroke* 17, 18–29.
- Feigin, V.L., Krishnamurthi, R.V., Parmar, P., Norrving, B., Mensah, G.A., Bennett, D.A., Barker-Collo, S., Moran, A.E., Sacco, R.L., Truelsen, T., Davis, S., Pandian, J.D., Naghavi, M., Forouzanfar, M.H., Nguyen, G., Johnson, C.O., Vos, T., Meretoja, A., Murray, C.J.L., Roth, G.A., GBD 2013 Writing Group, GBD 2013 Stroke Panel Experts Group, 2015. Update on the global burden of ischemic and hemorrhagic stroke in 1990-2013: The GBD 2013 study. *Neuroepidemiology* 45, 161–176.
- He, K., Chen, X., Xie, S., Li, Y., Dollár, P., Girshick, R., 2022. Masked autoencoders are scalable vision learners, in: *Proceedings of the IEEE/CVF conference on computer vision and pattern recognition*, pp. 16000–16009.
- Heo, T.S., Kim, Y.S., Choi, J.M., Jeong, Y.S., Seo, S.Y., Lee, J.H., Jeon, J.P., Kim, C., 2020. Prediction of stroke outcome using natural language processing-based machine learning of radiology report of brain mri. *Journal of personalized medicine* 10, 286.
- Hernandez Petzsche, M.R., de la Rosa, E., Hanning, U., Wiest, R., Valenzuela, W., Reyes, M., Meyer, M., Liew, S.L., Kofler, F., Ezhov, I., et al., 2022. Isles 2022: A multi-center magnetic resonance imaging stroke lesion segmentation dataset. *Scientific data* 9, 762.
- Herzog, L., Murina, E., Dürr, O., Wegener, S., Sick, B., 2020. Integrating uncertainty in deep neural networks for mri based stroke analysis. *Medical image analysis* 65, 101790.
- Hosny, A., Parmar, C., Quackenbush, J., Schwartz, L.H., Aerts, H.J.W.L., 2018. Artificial intelligence in radiology. *Nat. Rev. Cancer* 18, 500–510.
- Hu, E.J., Shen, Y., Wallis, P., Allen-Zhu, Z., Li, Y., Wang, S., Wang, L., Chen, W., 2021. LoRA: Low-Rank Adaptation of Large Language Models. *arXiv preprint arXiv:2106.09685*.
- Huo, F., Xu, W., Guo, J., Wang, H., Guo, S., 2024. C2kd: Bridging the modality gap for cross-modal knowledge distillation, in: *Proceedings of the IEEE/CVF Conference on Computer Vision and Pattern Recognition (CVPR)*, pp. 16006–16015.
- Izacard, G., Grave, E., 2021. Leveraging passage retrieval with generative models for open domain question answering, in: *Proceedings of the 16th Conference of the European Chapter of the Association for Computational Linguistics: Main Volume, ACL*. pp. 874–880.
- Jing, L., Tian, Y., 2020. Self-supervised visual feature learning with deep neural networks: A survey. *IEEE transactions on pattern analysis and machine intelligence* 43, 4037–4058.
- Karpukhin, V., Oguz, B., Min, S., Lewis, P., Wu, L., Edunov, S., ..., Yih, W.t., 2020. Dense passage retrieval for open-domain question answering, in: *Proceedings of the 2020 Conference on Empirical Methods in Natural Language Processing (EMNLP), ACL*. pp. 6769–6781.
- Ke, A., Ellsworth, W., Banerjee, O., Ng, A.Y., Rajpurkar, P., 2021. Chextransfer: performance and parameter efficiency of imagenet models for chest x-ray interpretation, in: *Proceedings of the Conference on Health, Inference, and Learning, Association for Computing Machinery, New York, NY, USA*. p. 116–124.
- Koska, I.O., Selver, A., Gelal, F., Uluc, M.E., Çetinoğlu, Y.K., Yurttutan, N., Serindere, M., Dicle, O., 2024. Deep learning classification of ischemic stroke territory on diffusion-weighted mri: Added value of augmenting the input with image transformations. *Journal of Imaging Informatics in Medicine*, 1–14.
- Lee, K.Y., Liu, C.C., Chen, D.Y.T., Weng, C.L., Chiu, H.W., Chiang, C.H., 2023a. Automatic detection and vascular territory classification of hyperacute staged ischemic stroke on diffusion weighted image using convolutional neural networks. *Scientific Reports* 13, 404.
- Lee, S., Kim, W.J., Ye, J.C., 2023b. Llm itself can read and generate cxr images. *arXiv preprint arXiv:2305.11490*.

- Lewis, P., Perez, E., Piktus, A., Petroni, F., Karpukhin, V., Goyal, N., Küttler, H., Lewis, M., Yih, W.t., Rocktäschel, T., et al., 2020. Retrieval-augmented generation for knowledge-intensive nlp tasks. *Advances in Neural Information Processing Systems* 33, 9459–9474.
- Li, C., Wong, C., Zhang, S., Usuyama, N., Liu, H., Yang, J., Naumann, T., Poon, H., Gao, J., 2024. Llava-med: Training a large language-and-vision assistant for biomedicine in one day. *Advances in Neural Information Processing Systems* 36.
- Liu, C.F., Zhao, Y., Yedavalli, V., Leigh, R., Falcao, V., STIR and VISTA Imaging investigators, Miller, M.I., Hillis, A.E., Faria, A.V., 2023. Automatic comprehensive radiological reports for clinical acute stroke MRIs. *Commun. Med. (Lond.)* 3, 95.
- Ma, W., Li, S., Cai, L., Kang, J., 2024. Learning modality knowledge alignment for cross-modality transfer. *arXiv preprint arXiv:2406.18864* .
- McDonald, R.J., Schwartz, K.M., Eckel, L.J., Diehn, F.E., Hunt, C.H., Bartholmai, B.J., Erickson, B.J., Kallmes, D.F., 2015. The effects of changes in utilization and technological advancements of cross-sectional imaging on radiologist workload. *Acad. Radiol.* 22, 1191–1198.
- Moor, M., Banerjee, O., Abad, Z.S.H., Krumholz, H.M., Leskovec, J., Topol, E.J., Rajpurkar, P., 2023. Foundation models for generalist medical artificial intelligence. *Nature* 616, 259–265.
- Mouridsen, K., Thurner, P., Zaharchuk, G., 2020. Artificial intelligence applications in stroke. *Stroke* 51, 2573–2579.
- Ong, C.J., Orfanoudaki, A., Zhang, R., Caprasse, F.P.M., Hutch, M., Ma, L., Fard, D., Balogun, O., Miller, M.I., Minnig, M., et al., 2020. Machine learning and natural language processing methods to identify ischemic stroke, acuity and location from radiology reports. *PloS one* 15, e0234908.
- Powers, W.J., Rabinstein, A.A., Ackerson, T., Adeoye, O.M., Bambakidis, N.C., Becker, K., Biller, J., Brown, M., Demaerschalk, B.M., Hoh, B., et al., 2019. Guidelines for the early management of patients with acute ischemic stroke: 2019 update to the 2018 guidelines for the early management of acute ischemic stroke: a guideline for healthcare professionals from the american heart association/american stroke association. *Stroke* 50, e344–e418.
- Ram, O., Eisenschlos, J., Ra, S., ..., 2023. Inference-time intervention for knowledge integration in generative models, in: *Proceedings of the 61st Annual Meeting of the Association for Computational Linguistics (ACL)*, ACL, pp. 5403–5418.
- San Román, L., Menon, B.K., Blasco, J., Hernández-Pérez, M., Dávalos, A., Majoie, C.B., Campbell, B.C., Guillemin, F., Lingsma, H., Anxionnat, R., et al., 2018. Imaging features and safety and efficacy of endovascular stroke treatment: a meta-analysis of individual patient-level data. *The Lancet Neurology* 17, 895–904.
- Singhal, K., Tu, T., Gottweis, J., Sayres, R., Wulczyn, E., Hou, L., Clark, K., Pfohl, S., Cole-Lewis, H., Neal, D., et al., 2023. Towards expert-level medical question answering with large language models. *arXiv preprint arXiv:2305.09617* .
- Tasci, B., Tasci, I., 2022. Deep feature extraction based brain image classification model using preprocessed images: Pdrnet. *Biomedical Signal Processing and Control* 78, 103948.
- The National Institute of Neurological Disorders and Stroke rt-PA Stroke Study Group, 1995. Tissue plasminogen activator for acute ischemic stroke. *New England Journal of Medicine* 333, 1581–1588.
- Wardlaw, J.M., Smith, C., Dichgans, M., 2019. Small vessel disease: mechanisms and clinical implications. *Lancet Neurol.* 18, 684–696.
- Xie, Z., Zhang, Z., Cao, Y., Lin, Y., Bao, J., Yao, Z., Dai, Q., Hu, H., 2022. Simmim: A simple framework for masked image modeling, in: *Proceedings of the IEEE/CVF Conference on Computer Vision and Pattern Recognition*, pp. 9653–9663.
- Xiong, Y., Campbell, B.C., Schwamm, L.H., Meng, X., Jin, A., Parsons, M.W., Fisher, M., Jiang, Y., Che, F., Wang, L., Zhou, L., Dai, H., Liu, X., Pan, Y., Duan, C., Xu, Y., Xu, A., Zong, L., Tan, Z., Ye, W., Wang, H.,

Wang, Z., Hao, M., Cao, Z., Wang, L., Wu, S., Li, H., Li, Z., Zhao, X., Wang, Y., 2024. Tenecteplase for ischemic stroke at 4.5 to 24 hours without thrombectomy. *New England Journal of Medicine* 391, 203–212.

Zhou, L., Liu, H., Bae, J., He, J., Samaras, D., Prasanna, P., 2023. Self pre-training with masked autoencoders for medical image classification and segmentation, in: *2023 IEEE 20th International Symposium on Biomedical Imaging (ISBI)*, IEEE. pp. 1–6.